

Gravitational lensing

Olaf Wucknitz^{*†}

Joint Institute for VLBI in Europe, Dwingeloo, Netherlands

E-mail: wucknitz@astro.uni-bonn.de

This is a short and biased review of gravitational lensing with emphasis on the radio and especially VLBI aspects. We briefly explain the basic idea and give a short sketch of the discovery of the first lens before we more systematically discuss the general fields that can be studied with lensing. We intentionally omit the details the average lensing expert would like to see and instead try to give a very general overview addressed to the radio astronomer working in some other field. The lens B0218+357 is presented as an example to show many aspects of lensing in a case that already has led to interesting results but still has additional potential for the future.

*8th European VLBI Network Symposium
September 26-29, 2006
Toruń, Poland*

^{*}Speaker.

[†]Current address: Argelander-Institut für Astronomie, Universität Bonn, Germany

1. The idea

The idea that gravity might influence the propagation of light is much older than the EVN or even radio astronomy. Even Newton (1704) mentioned the possibility¹, but without going into any details. Henry Cavendish was the first to calculate deflections using the simplified model that light consists of classical particles moving with the speed of light, thus being weakly deflected in a gravitational field (see Will, 1988). Without knowing of this unpublished work, Soldner (1801) used a similar concept and wrote the first article about gravitational lensing. He found that the deflection angle (see Fig. 1) between the asymptotic light paths before and after an encounter with a mass M at a distance r is $\alpha = 2GM/(c^2r)$, where G and c are the gravitational constant and the speed of light, respectively. Before developing the theory of general relativity, Einstein (1911) used another approach that does not rely on the incorrect classical model of light but, instead, used the principle of equivalence to find the same result as Soldner. A few years later, our still best theory of gravitation was finished and Einstein (1915) could reconsider the deflection of light, finding that it should be *twice* as large as in non-relativistic theory:

$$\alpha = \frac{4GM}{c^2r} \quad (1.1)$$

This result was confirmed (with limited accuracy) by Eddington (1919), who determined the deflection of light caused by the Sun by measuring positions of stars close to its limb during a solar eclipse. This served as a first independent test of the new theory.

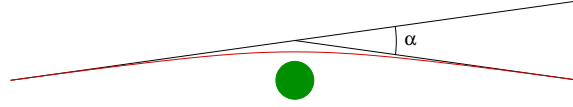


Figure 1: Light deflection

Almost all aspects of gravitational lensing theory can be derived from Eq. (1.1), together with the astrophysical background that is required to relate it to observable quantities. It is easy to see that in the presence of sufficiently large and compact masses, situations are possible where light from a background source reaches the observer along different light paths, which are then interpreted as multiple images of this source. Typical lenses show two or four images, which in very symmetrical systems merge to form rings around the lens, the so-called Einstein rings.

2. The first lensed double: 0957+561

This radio source (without knowing about its lensed nature at that time) was discovered in a 966-MHz survey made with the Jodrell Bank MkIA telescope. One of the sources in that survey, 0958+56, was a blend of the spiral galaxy NGC 3079 with the new source 0957+561. The latter had an optical identification as two point-like images with a separation of about $6''$ (Porcas et al., 1980, and Fig. 2, left).

¹“Do not bodies act upon light at a distance, and by their action bend its rays; and is not this action strongest at the least distance?”

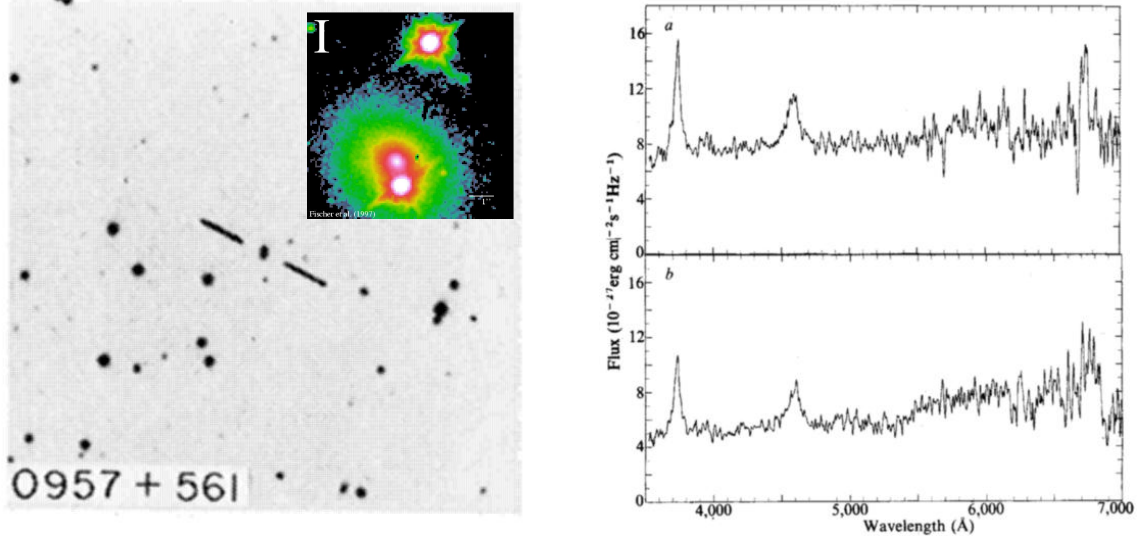


Figure 2: Left: Optical POSS image and identification of 0957+561 (from Porcas et al., 1980). Inset: HST I image (from Kochanek et al., 2006) showing the two images *A* and *B* and the lensing galaxy *G* close to *B*. Right: Spectra of both images (from Walsh et al., 1979)

Optical spectra of the two images appeared like almost identical copies of a QSO spectrum with a redshift of $z = 1.4$. Since a chance alignment of so similar objects with such a close separation is extremely unlikely, the favoured interpretation was (and still is) that we see two gravitationally lensed images of one and the same source (Walsh et al., 1979). Many interesting (and amusing) details of the first discovery, including a description of all coincidences that had to conspire to allow the success, are described by Walsh (1989).

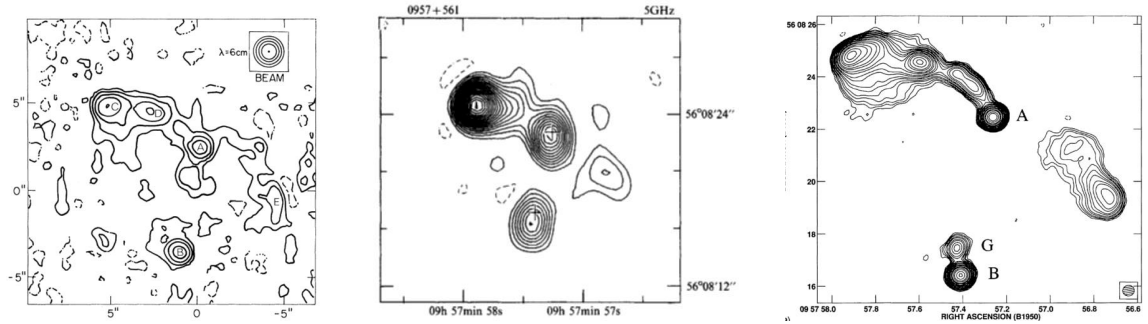


Figure 3: Interferometric observations of 0957+561 at 6 cm. Left: early VLA (Roberts et al., 1979). Centre: Cambridge 5 km. Right: full VLA (Harvanek et al., 1997).

Doubts were expressed by Roberts et al. (1979) when first interferometric observations showed the complicated structure of the double radio source (see Fig. 3). The *A* image seems to show a jet and radio lobes and one could naively expect that the same should be true for *B* if both are really lensed images of one source. In the maps, on the other hand, image *B* looks perfectly point-like. However, Fig. 4 illustrates how different parts of the source may well be lensed with different multiplicity. The specific situation for 0957+561 is shown in Fig. 5.

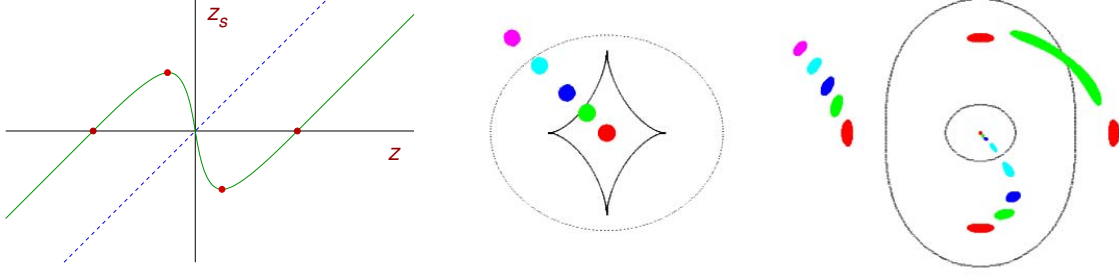


Figure 4: Left: Illustration of a typical lens mapping in one dimension, showing the true source position z_s as a function of the apparent image position z . For source positions far away from the origin, we see only one image. When the source crosses the extrema of the curve, two additional images appear or disappear. Centre and right: Illustration of this effect in two dimensions. The central panel shows the source plane with the caustic curves, the right one the image plane with the corresponding critical curves. These curves correspond to the red dots in the left panel. Whenever the source crosses one of the curves, two merging images (dis)appear. At this moment, the images are magnified extremely.

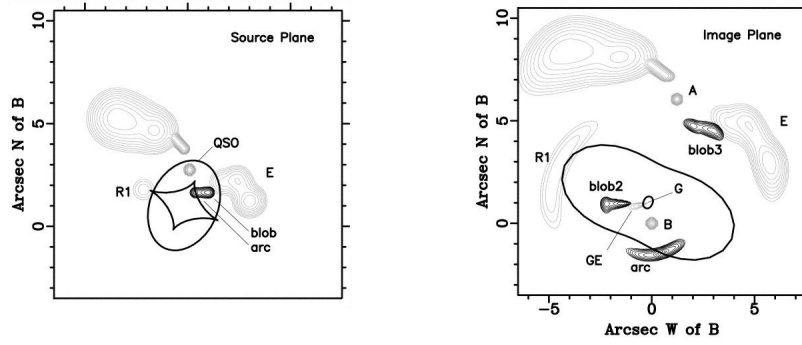


Figure 5: Schematic source plane (left) and image plane (right) of 0957+561. Shown are caustics/critical curves, radio contours in grey and optical contours in black. We see two images of the core but only one image of the extended radio jet and lobes. (from Avruch et al., 1997)

3. First VLBI observations of lenses

Naturally, the first discovered lens was also the first target for VLBI observations (Fig. 6). In the fringe-rate spectrum, we see two peaks corresponding to the two images *A* and *B*, which thus both must have compact structure on scales below 20 mas. The first multi-component model fits show that both images have a very similar structure, consisting of a compact core component and an elongated feature that probably corresponds to a jet. These jets show many details in VLBI maps produced later.

It is impressive to see how far VLBI has evolved from simple fringe-rate spectrum plots to detailed maps of gravitational lenses. The first observations also show that real science can be done with only one VLBI baseline.

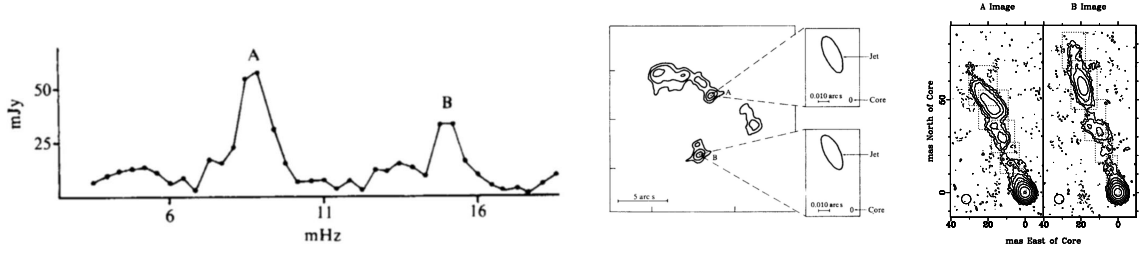


Figure 6: Left: Residual fringe rate spectrum of 0957+561 from the first VLBI observations; 20-min integration, Effelsberg-Jodrell baseline (from Porcas et al., 1979). Centre: First Gaussian model fit results (from Porcas et al., 1981). Right: Later detailed maps for comparison (from Campbell et al., 1995).

4. Fields of study

After this introduction, we come to a more systematic discussion of the several topics that can be studied with gravitational lensing. Fig. 7 schematically shows a typical lensing scenario with multiple images of one source.

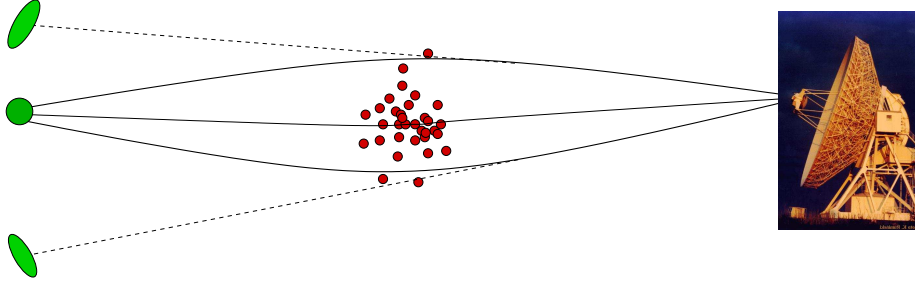


Figure 7: Lensing can be used to study the lensed sources (left), the lenses themselves (centre), propagation effects and extinction (anywhere between source and observer), and the properties of global spacetime (including cosmology and tests of relativity.)

4.1 Lenses as natural telescopes

The lens effect can be utilised to extend the capabilities of our instruments because it provides additional magnification and corresponding flux amplification, and in this way boosts the effective resolution and sensitivity of observations. Clusters of galaxies provide the largest lensing cross-sections and are thus the primary of these *natural telescopes*. Two examples are shown in Figs. 8 and 9. In one case, the amplification made it possible to detect a distant galaxy at $z = 7$ and observe its optical spectrum. In the others, the lensing amplification enhances weak, background star-forming galaxies that have first been found at sub-mm wavelength above the radio detection limit. Without the lenses, current radio telescopes would not be sufficiently sensitive to study these objects at all.

In galaxy-scale lenses, the regions of high amplifications are very small, but in rare occasions it happens that a radio source is located so close to a caustic that it is amplified by factors of a few hundred. B2016+112 is one of those examples. In another talk at this meeting, More & Porcas (2006) present new HSA observations of this system, showing source components almost merging

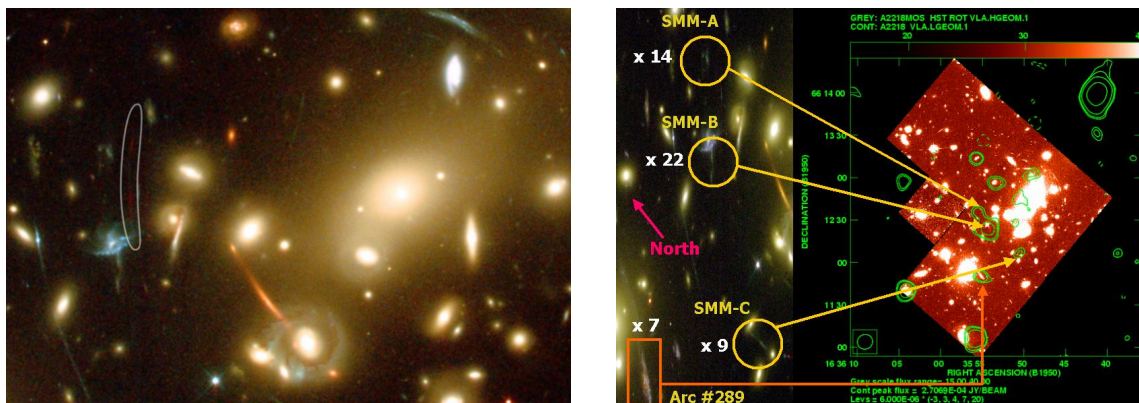


Figure 8: The lensing cluster of galaxies A2218. Left: A $z = 7$ background galaxy amplified by a factor of $\mu \approx 25$ (from Kneib et al., 2004). Right: The first radio detection of a lensed star-forming galaxy (from Garrett et al., 2005).

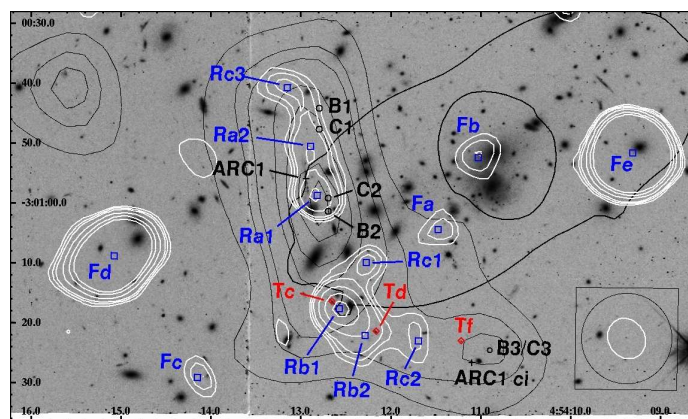


Figure 9: The cluster MS0451.6–0305 shows a number of lensed background source components in the radio (white contours) and sub-mm (black contours) domains. Lens models predict that they all form a compact ensemble of forming or merging galaxies at high redshift. (from Berciano Alba et al., 2007)

at the critical curve with extreme magnifications. Back-projecting these components into the source plane will in the future provide μarcsec -resolution maps of this source.

4.2 Mass distributions of lenses

Studying the mass distributions of lenses is one of the most important fields in lensing research for several reasons. On one hand, the mass distribution governs the light deflection and image configuration, including magnifications. Without a good knowledge of these properties, applications of lenses as natural telescopes (or for other purposes) would become inaccurate and speculative.

However, this argument can be turned around and we can use the image configuration to constrain the mass distribution of the lens. This method provides the most accurate information about the mass distributions of very distant lenses, allowing the study of structure and evolution of galaxies in a systematic way. The standard approach to do this is to assume a simple parametrised mass distribution for the lens and make simple assumptions for the source structure, e.g. assume

that it consists of a small number of compact components. The model parameters (of the lens and source) are then varied in a way to fit the predicted image configuration to the observed one. This can include image positions as well as shapes of compact but slightly extended components. Generally, it is advantageous to have many lensed source components, but they have to be of a sufficiently simple structure to make this standard approach viable.

Fig. 10 illustrates this for the case of 0957+561, where the source is complicated enough to make this procedure a non-trivial task. The constraints are quite good, but unfortunately the structure of the lens (which consists of a massive cD galaxy together with its surrounding cluster) is so complicated that even these constraints are not sufficient to provide a good accuracy for the lens mass distribution. One disadvantage is that all the jet components are located very close to each other so that they sample the light deflection only in small regions, basically providing the deflection angle and its derivatives at only two points.

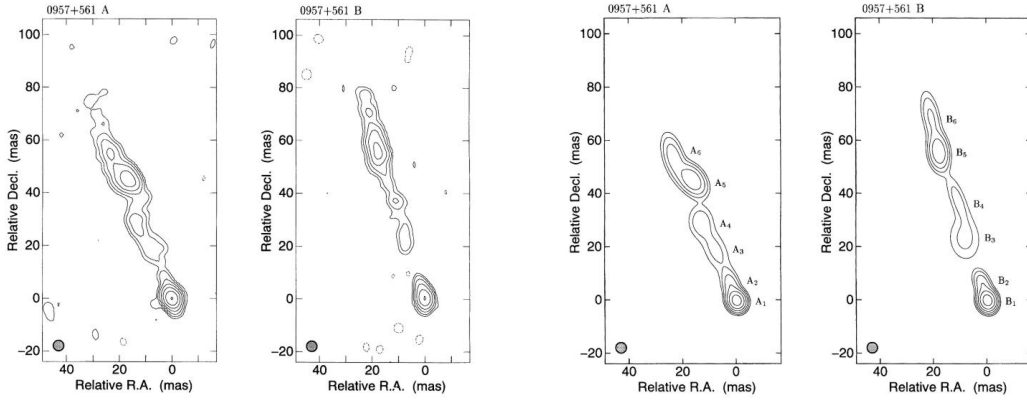


Figure 10: Constraints from the substructure of both jet images in 0957+561. The observed structure (left panels) of the jet images is parametrised as a collection of Gaussian model components (right panels). The parameters of these components are then used to determine a relative magnification matrix that linearly maps the central region of image *A* to *B* or vice versa. The mass-model parameters are then varied to fit the predicted matrix to the one determined from the observations. (from Garrett et al., 1994)

In order to obtain more information about the global properties of the mass distribution, it is necessary to have images at widely separated positions, especially at different distances from the lens centre. B1933+503 is a unique lens system consisting of *ten* images of several source components (see Fig. 11). Parametrised model fits (Cohn et al., 2001) for this system show that the mass distribution must be very close to isothermal (projected surface mass density $\sigma \propto 1/r$), a property found in most accurately modelled lenses. Later on, we will discuss how to use lensed general *extended* sources to constrain lens models.

The lensed image configuration not only provides information about the global mass distribution but is also sensitive for small-scale deviations as predicted by CDM structure-formation scenarios. Fig. 12 shows an example where each of the four images consists of three subcomponents. The general four-image geometry can be fitted well with smooth mass distributions, but these models cannot explain the relative positions of all subcomponents in the images. An easy explanation would be the presence of a small-mass clump close to one of the images that distorts the geometry very locally without affecting the global configuration. There are other cases where it is not the

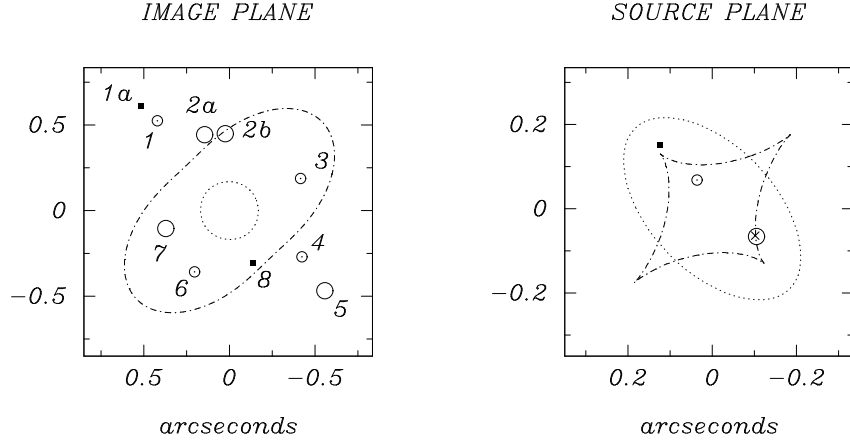


Figure 11: The lens B1933+503. Left: Image configuration with critical curves. Right: Source component configuration with caustics. One component (black dot) is doubly imaged, the other two (circles) are both quadruply imaged, resulting in ten images of these three components. The images probe the lensing potential at a wide range of radii. (from Nair, 1998)

image configuration but the flux density ratios that are in conflict with simple models. This is not surprising since small-scale mass substructure influences derivatives of deflection (determining the amplifications) much stronger than the deflections (and image positions) themselves.

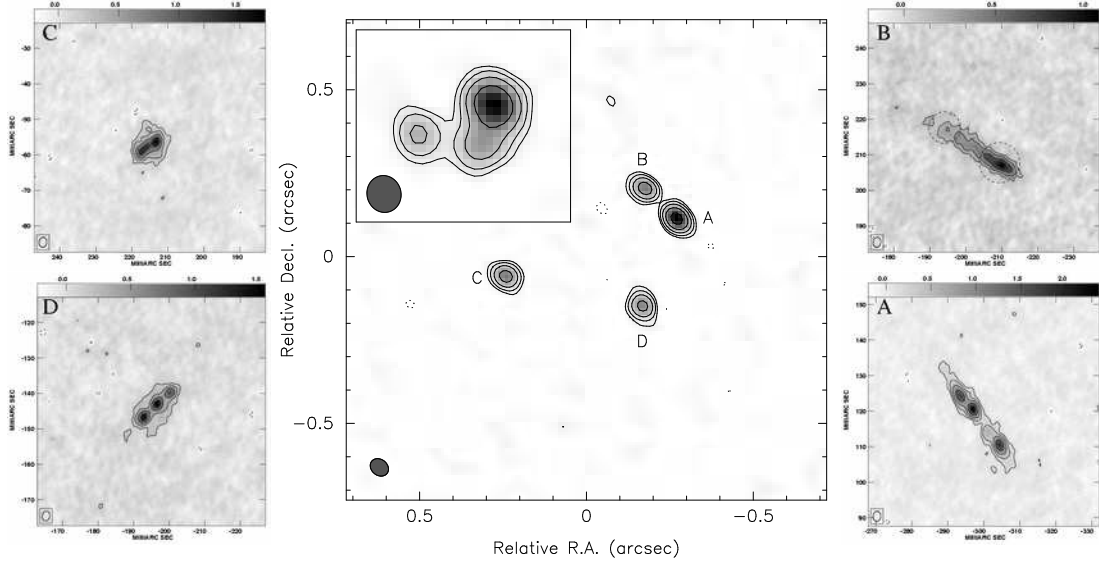


Figure 12: The quadruple lens system B0128+437. Centre: MERLIN map of the complete system (from Phillips et al., 2000). Outer fields: High-resolution VLBI maps of the four images (from Biggs et al., 2004).

Another aspect of the small-scale mass distribution that can be studied with lensing is the mass profile in the very centres of lensing galaxies. For a smooth mass profile with a non-diverging deflection angle, one would always expect an odd number of images, one of which would be located close to the lens centre. However, if the central mass concentration becomes very steep or even singular, this central image will be highly de-magnified or even completely suppressed.

Currently, only one such central image is believed to be detected (see Fig. 13, together with a case with no central image). Instead, there is evidence that isothermality of the mass profile typically extends very close to the lens galaxy centres, which would suppress the central images. There is no good explanation for this fact in standard structure-formation theories.

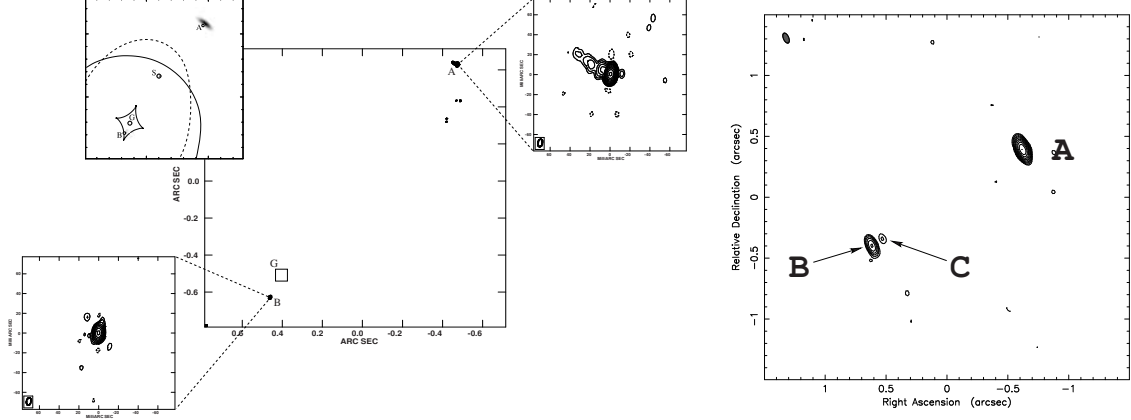


Figure 13: Two cases of studies concerning possible central images. Left: B1030+074, where even with HSA observations no central image could be found (from Zhang et al., 2007). Right: J1632–0033, the currently most (and maybe only) convincing case with a weak central image (from Winn et al., 2003).

4.3 Propagation effects: scattering, absorption etc.

The study of propagation effects like scatter broadening, free-free absorption or extinction and reddening in the optical domain is usually plagued by the lack of knowledge of the *intrinsic* structure and spectral energy distribution of a distant source, with which the *observed* properties could be compared. Gravitational lensing kindly produces two or more copies of the same source component that are identical in their spectra and have only simple (and easy to model) differences in their total flux density and source structure. By comparing properties of these images, one can directly infer the *differential* propagation effects like differential reddening or differential scatter broadening, without assumptions about the intrinsic properties. This will be shown for one example later.

4.4 Measurement of distances and cosmology

Long before the discovery of the first lens, it was argued by Refsdal (1964, 1966) that the lens effect can be used to test cosmological theories and to measure distances and thus the Hubble constant in particular. The principle behind this idea is very simple. In a typical lens system, we can measure the angular separations between the observed images and the lens. Modelling the mass distribution then gives us all the other angles defining the geometry (like the true source position). Ratios of distances between observer, lens and source can be derived easily from the observed redshifts. We conclude that in such a situation the complete lensing geometry is known, *except for the scale*. If only one length in the system can be measured, all other lengths, including the distances to the lens and source, can immediately be calculated. It was the idea of Refsdal (1964) that the light travel-times will differ from image to image (because of different geometrical paths

and different Shapiro delays) and that this light travel-time difference can be used as the defining length to scale the whole geometry. If the background source is variable, these variations will be seen in all the images, but shifted relative to each other by the corresponding time delays. Once the distances are determined, they can be used together with the redshifts to estimate the Hubble constant. Distances for given redshifts are inversely proportional to the Hubble constant, and the time delay is proportional to the distances, so that the product $H_0\Delta t$ is a constant that can be derived from the lens mass model, which, in turn, is constrained by the image geometry. This method has been applied to a number of lens systems, leading to more or less consistent results. We will discuss only one example further below.

4.5 Tests of relativity

The most fundamental test of relativity performed with the lens effect consists of measuring the deflection angle in our solar system and comparing it with the theoretical expectations. For this purpose the deflection can be parametrised as

$$\alpha = 2(1 + \gamma) \frac{GM}{c^2 r}$$

and the resulting γ can be measured. Two special values would be $\gamma = 0$ as expected from Newtonian theory and $\gamma = 1$ as expected from general relativity. The work of Eddington (1919) was only a first example, and the accuracy has improved by several orders of magnitude by using VLBI techniques. Shapiro et al. (2004) found $\gamma = 0.9998 \pm 0.0004$ from a combination of very many geodetic VLBI data sets, which confirms general relativity with high accuracy.

It has also been claimed that the deflection of light by a moving object (Jupiter in this case) can be used to measure the propagation speed of gravity (Kopeikin, 2001). Such an experiment has actually been carried out (Fomalont & Kopeikin, 2003), and the outcome is consistent with relativity. However, there are serious arguments against this interpretation of the experiment (see e.g. Will, 2003; Carlip, 2004) and the debate has not led to an agreement between the opponents yet.

5. The lens B0218+357

This lens system is one of the best studied cases and is a good example for many of the applications of the lens effect discussed above. It consists of two bright images and an additional Einstein ring with the same diameter as the image separation (Fig. 14). The two images are resolved by VLBI and show the core and inner jet of the lensed background source (e.g. Biggs et al., 2003).

5.1 Lens models and Hubble constant

B0218+357 has some unique properties that make it particularly well suited to determine the Hubble constant using Refsdal's method. Firstly, the time delay is known with sufficient accuracy. Biggs et al. (1999) find $\Delta T = (10.5 \pm 0.4)$ d, a result that is consistent with that of Cohen et al. (2000). Secondly, the lens is an isolated spiral galaxy without close neighbours or clusters nearby, which allows the use of simple models with a small number of parameters as a realistic description. Finally, the wealth of structure in the Einstein ring and the VLBI maps of the lensed jets provides

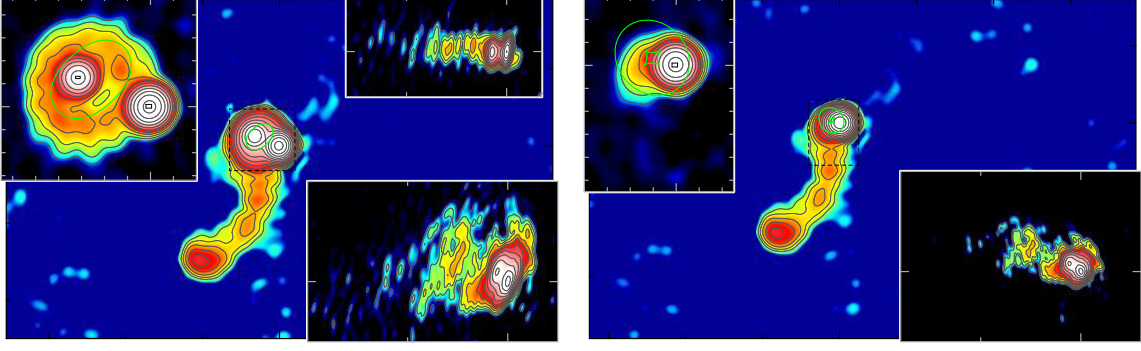


Figure 14: The lens B0218+357. Left: The lens plane as we see it. The central map provides an overview. The Einstein ring and the two images are shown in the upper left; the insets at the right show the magnified VLBI substructure of the two images. The magnified regions are marked by black rectangles. Right: The reconstructed (unlensed) source plane. (from Wucknitz et al., 2004)

a good number of valuable constraints for the modelling. The VLBI substructure is especially sensitive to the radial mass profile, which seems to be very close to isothermal but slightly shallower (Biggs et al., 2003). Unfortunately, the accurate lens position (relative to the images) was not known until recently. The image separation is only 330 mas, the smallest of all galaxy lenses, which makes direct optical measurements very difficult. However, the structure of the Einstein ring can be used to determine the lens position indirectly. Contrary to the lens modelling methods described before, the source cannot be described as a small number of point-like sources anymore. Instead, more sophisticated methods must be used, in which the true source structure is also fitted for in a non-parametric way.

We used our own improved version of the LensClean algorithm to accomplish this task (Wucknitz, 2004). LensClean iteratively builds a source model similarly to the normal Clean algorithm, but takes into account the effect of the (for the moment fixed) lens model. ‘Clean components’ are allowed only in combinations that are consistent with the effect of the lens. If, for example, a component is to be included at a position that is quadruply imaged, all four lensed images have to be included in the model, scaled with their respective amplifications. Once converged, this inner loop of LensClean has determined a source model that minimises the residuals given a certain lens model. An outer loop then varies the lens model parameters, again in order to minimise the residuals. The final result is a simultaneous fit of lens and source model. The main result in the case of B0218+357 is the lens position, which then directly translates to a value for the Hubble constant (Wucknitz et al., 2004):

$$H_0 = (78 \pm 6) \text{ km s}^{-1} \text{ Mpc}^{-1}$$

The lens position was later confirmed by a direct optical measurement using the HST/ACS (York et al., 2005). The result for H_0 is consistent with other methods that use completely independent information. Because it is determined by a direct one-step method, the systematic uncertainties inherent in the complex distance-ladder methods are avoided.

5.2 Propagation effects

It has been known for long that the flux density ratio of the two images A/B shows a strong

frequency dependence. At high frequencies, it is close to 4 and decreases for lower frequencies. This is surprising since lensing is achromatic and should not change the spectra of the images. One possible explanation would be source shifts as a function of frequency, which, together with the strong magnification gradient, could explain the observed trend, provided they were of the order 10 mas or more. Mittal et al. (2006a) investigated this possibility by measuring the image positions with multi-frequency, phase-referencing VLBI observations. They found (see Fig. 15) that any image shifts are of the order of 1 mas or less, not enough to explain the observed effect. Similarly, changes of the source structure could be ruled out as reason for the changing flux density ratios. The most plausible explanation is a free-free absorption, mainly in the *A* image.

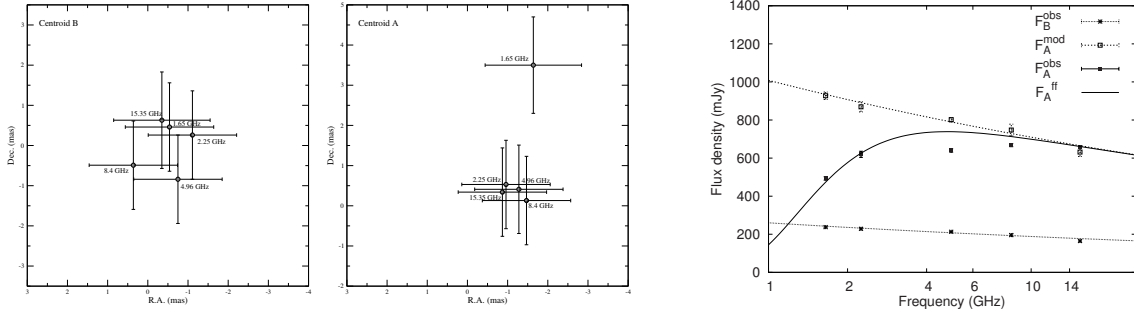


Figure 15: Left: Image positions of *A* and *B* for different frequencies (from Mittal et al., 2006a). Right: free-free absorption model for the flux density of *A* derived from *B* (F_A^{ff}) with corresponding measurements (F_A^{obs}). The agreement is not perfect but reasonably good (from Mittal et al., 2007).

5.3 More VLBI aspects

It should be noted that B0218+357 was the target of the first real-time EVN observations in 2004. The map from this small data set is shown in Fig. 16 (left). Currently, the author is working on the analysis of a 90-cm VLBI experiment conducted recently. The goal was to map more details in the Einstein ring and to obtain more information about propagation effects that are strongest at lower frequencies. Fig. 16 (right) shows a very preliminary map compared to a VLA+Pie Town map at 2-cm. Two additional correlator passes of the same 90-cm observations are used for a wide-field mapping experiment that constitutes the first wide-field VLBI mini-survey to study the high-resolution radio sky at such low frequencies. First results are presented by Lenc et al. (2006) at this conference. See also Lenc et al. (2007).

6. Outlook

Like many other fields, gravitational lens research takes advantage of the technical progress in radio astronomy and particularly in VLBI. The EVN grows continuously, providing steadily improving *uv* coverage, mapping quality and resolution. Higher bandwidths provide the increasing sensitivity that is needed to map more extended source components with high quality. Such future VLBI experiments will lead to more accurate lens mass models than currently available. This development is complemented by the upgraded EVLA and *e*-MERLIN that will come online soon. All these arrays will allow the mapping of even weaker structures on scales of the image splitting

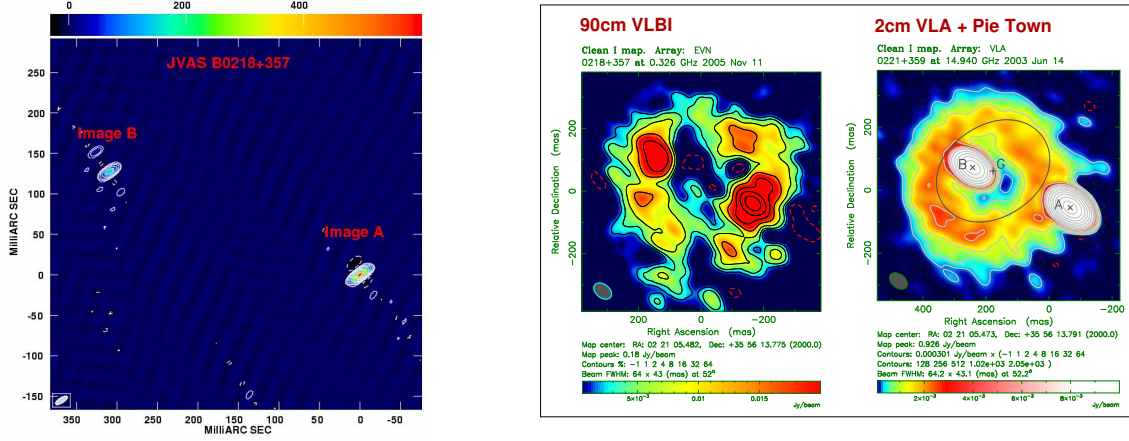


Figure 16: Left: The first real-time EVN image produced at JIVE. Right: Preliminary 90-cm VLBI map in comparison with a 2-cm VLA+Pie Town map. This is shown only for illustration, the calibration is still very poor at this stage.

with sufficient resolution to utilise the information such sources provide for mass models and other purposes. It will finally be possible to map even normal star-forming galaxies in great detail. Such lensed sources have such a wealth of smaller structures (Fig. 17) that they allow a detailed mapping of the lensing potential and thus the mass distribution of lensing galaxies.

EVLA, *e*-MERLIN, and above all LOFAR (with extended baselines) will allow future lens surveys that increase the number of radio lenses by at least an order of magnitude. This development has to be supplemented by the development of new analysis techniques that can extract all information from current and future observations. LensClean can only be one first step in this direction.

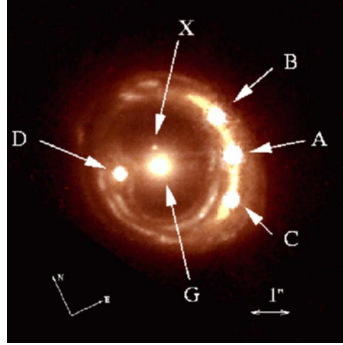


Figure 17: Radio astronomy has to compete with this! Shown is the lensed star-burst galaxy J1131-1231 in the optical domain (from Claeskens et al., 2006). Future radio telescopes will map such sources with even better quality than shown in this HST image. Each lensed star-forming region will provide its own constraints on the mass distribution of the lens.

7. Summary

We have discussed how the lens effect can be used to study all aspects of the lensing situation. We use the lens as a natural telescope to study the sources in greater detail, we determine the mass

distributions of high-redshift lens galaxies, and can even determine the Hubble constant and do cosmology. Additionally, lenses provide us with (almost) identical copies of lensed sources that can then be used to study differential propagation effects like scattering or absorption.

Radio observations are particularly useful for several reasons. Firstly, radio interferometers span the largest range of possible resolutions down to the sub-mas level. Secondly, the effects of microlensing and extinction, that make the interpretation of optical observations very difficult, can mostly be avoided at radio wavelengths. Instead of asking what radio astronomy can do for lensing, we can also ask what lensing can do for radio astronomy. It is our hope that the further development of deconvolution methods for the lensed situation will also provide new and better algorithms for a general use. Such a trigger for new developments should be very welcome.

Finally, we have to add that this review covers only a small subset of relevant topics in gravitational lens research. Other important subjects like microlensing, weak lensing, lensing surveys, measuring time delays, and a number of very interesting lens systems have not been mentioned at all. That does not imply that those fields are less exciting.

Acknowledgments

This work was supported by the European Community's Sixth Framework Marie Curie Research Training Network Programme, Contract No. MRTN-CT-2004-505183 "ANGLES".

References

- Avruch, I. M., Cohen, A. S., Lehar, J., Conner, S. R., Haarsma, D. B. & Burke, B. F.: 1997, *Low surface brightness radio structure in the field of gravitational lens 0957+561*, ApJ 488, L121.
- Berciano Alba, A., Garrett, M. A., Koopmans, L. V. E. & Wucknitz, O.: 2007, *Highly-magnified, multiply-imaged radio counterparts of the sub-mm starburst emission in the cluster-lens MS0451.6-0305*, A&A 462, 903.
- Biggs, A. D., Browne, I. W. A., Helbig, P., Koopmans, L. V. E., Wilkinson, P. N. & Perley, R. A.: 1999, *Time delay for the gravitational lens system B0218+357*, MNRAS 304, 349.
- Biggs, A. D., Browne, I. W. A., Jackson, N. J., York, T., Norbury, M. A., McKean, J. P. & Phillips, P. M.: 2004, *Radio, optical and infrared observations of CLASS B0128+437*, MNRAS 350, 949.
- Biggs, A. D., Wucknitz, O., Porcas, R. W., Browne, I. W. A., Jackson, N. J., Mao, S. & Wilkinson, P. N.: 2003, *Global 8.4-GHz VLBI observations of JVAS B0218+357*, MNRAS 338, 599.
- Campbell, R. M., Lehar, J., Corey, B. E., Shapiro, I. I. & Falco, E. E.: 1995, *VLBI observations of the gravitational lens system 0957+561*, AJ 110, 2566.
- Carlip, S.: 2004, *Model-dependence of Shapiro time delay and the 'speed of gravity/speed of light' controversy*, Classical and Quantum Gravity 21, 3803.
- Claeskens, J.-F., Sluse, D., Riaud, P. & Surdej, J.: 2006, *Multi wavelength study of the gravitational lens system RXS J1131-1231. II. Lens model and source reconstruction*, A&A 451, 865.
- Cohen, A. S., Hewitt, J. N., Moore, C. B. & Haarsma, D. B.: 2000, *Further investigation of the time delay, magnification ratios, and variability in the gravitational lens 0218+357*, ApJ 545, 578.

- Cohn, J. D., Kochanek, C. S., McLeod, B. A. & Keeton, C. R.: 2001, *Constraints on galaxy density profiles from strong gravitational lensing: the case of B1933+503*, ApJ 554, 1216.
- Eddington, A. S.: 1919, *The total eclipse of 1919 May 29 and the influence of gravitation on light*, The Observatory 42, 119.
- Einstein, A.: 1911, *Über den Einfluß der Schwerkraft auf die Ausbreitung des Lichtes*, Ann. Physik 35, 898.
- Einstein, A.: 1915, *Erklärung der Perihelbewegung des Merkur aus der allgemeinen Relativitätstheorie*, Sitzungsber. Preuß. Akad. Wissensch., erster Halbband, p. 831.
- Fomalont, E. B. & Kopeikin, S. M.: 2003, *The measurement of the light deflection from Jupiter: experimental results*, ApJ 598, 704.
- Garrett, M. A., Calder, R. J., Porcas, R. W., King, L. J., Walsh, D. & Wilkinson, P. N.: 1994, *Global VLBI observations of the gravitational lens system 0957+561A, B*, MNRAS 270, 457.
- Garrett, M. A., Knudsen, K. K. & van der Werf, P. P.: 2005, *Gravitationally lensed radio emission associated with SMM J16359+6612, a multiply imaged submillimeter galaxy behind A 2218*, A&A 431, L21.
- Harvanek, M., Stocke, J. T., Morse, J. A. & Rhee, G.: 1997, *High dynamic range VLA observations of the gravitationally lensed quasar 0957+561*, AJ 114, 2240.
- Kneib, J.-P., Ellis, R. S., Santos, M. R. & Richard, J.: 2004, *A probable $z \sim 7$ galaxy strongly lensed by the rich cluster A2218: exploring the dark ages*, ApJ 607, 697.
- Kochanek, C. S., Falco, E. E., Impey, C., Lehár, J., McLeod, B. & Rix, H.-W.: 2006, *CASTLeS website*, <http://cfa-www.harvard.edu/castles/>.
- Kopeikin, S. M.: 2001, *Testing the relativistic effect of the propagation of gravity by Very Long Baseline Interferometry*, ApJ 556, L1.
- Lenc, E., Garrett, M., Wucknitz, O., Anderson, J. & Tingay, S.: 2006, *Living life on the edge – Widefield VLBI at 90 cm!*, proceedings of the 8th European VLBI symposium, PoS (8thEVN) 079.
- Lenc, E., Garrett, M., Wucknitz, O., Anderson, J. & Tingay, S.: 2007, *A deep, high resolution survey of the low frequency radio sky*, ApJ. in print.
- Mittal, R., Porcas, R. & Wucknitz, O.: 2007, *Free-free absorption in the gravitational lens JVAS B0218+357*, A&A 465, 405.
- Mittal, R., Porcas, R., Wucknitz, O., Biggs, A. & Browne, I.: 2006a, *VLBI phase-reference observations of the gravitational lens JVAS B0218+357*, A&A 447, 515.
- More, A. & Porcas, R.: 2006, *Multi-frequency VLBI observations of the gravitational lens B2016+112*, proceedings of the 8th European VLBI symposium, PoS (8thEVN) 030.
- Nair, S.: 1998, *Modelling the 10-image lensed system B1933+503*, MNRAS 301, 315.
- Newton, I.: 1704, *Opticks*.
- Phillips, P. M., Norbury, M. A., Koopmans, L. V. E., Browne, I. W. A., Jackson, N. J., Wilkinson, P. N., Biggs, A. D., Blandford, R. D., de Bruyn, A. G., Fassnacht, C. D., Helbig, P., Mao, S.,

- Marlow, D. R., Myers, S. T., Pearson, T. J., Readhead, A. C. S., Rusin, D. & Xanthopoulos, E.: 2000, *A new quadruple gravitational lens system: CLASS B0128+437*, MNRAS 319, L7.
- Porcas, R. W., Booth, R. S., Browne, I. W. A., Walsh, D. & Wilkinson, P. N.: 1979, *VLBI observations of the double QSO, 0957 + 561 A, B*, Nature 282, 385.
- Porcas, R. W., Booth, R. S., Browne, I. W. A., Walsh, D. & Wilkinson, P. N.: 1981, *VLBI structures of the images of the double QSO 0957+561*, Nature 289, 758.
- Porcas, R. W., Urry, C. M., Browne, I. W. A., Cohen, A. M., Daintree, E. J. & Walsh, D.: 1980, *Radio positions and optical identifications for radio sources selected at 966 MHz. II*, MNRAS 191, 607.
- Refsdal, S.: 1964, *On the possibility of determining Hubble's parameter and the masses of galaxies from the gravitational lens effect*, MNRAS 128, 307.
- Refsdal, S.: 1966, *On the possibility of testing cosmological theories from the gravitational lens effect*, MNRAS 132, 101.
- Roberts, D. H., Greenfield, P. E. & Burke, B. F.: 1979, *The double quasar 0957+561 — A radio study at 6-centimeters wavelength*, Science 205, 894.
- Shapiro, S. S., Davis, J. L., Lebach, D. E. & Gregory, J. S.: 2004, *Measurement of the solar gravitational deflection of radio waves using geodetic Very-Long-Baseline Interferometry data, 1979–1999*, Phys. Rev. Lett. 92, 121101.
- Soldner, J.: 1801, *Über die Ablenkung eines Lichtstrahls von seiner geradlinigen Bewegung durch die Attraktion eines Weltkörpers, an welchem er nahe vorbeigeht*, Berliner Astron. Jahrb. 1804, Späten, p. 161.
- Walsh, D.: 1989, *0957 + 561: the unpublished story*, in J. M. Moran, J. N. Hewitt & K.-Y. Lo (eds), *LNP Vol. 330: Gravitational Lenses*, Springer, p. 11.
- Walsh, D., Carswell, R. F. & Weymann, R. J.: 1979, *0957 + 561 A, B — Twin quasistellar objects or gravitational lens*, Nature 279, 381.
- Will, C. M.: 1988, *Henry Cavendish, Johann von Soldner, and the deflection of light*, Am. J. Phys. 56, 413.
- Will, C. M.: 2003, *Propagation speed of gravity and the relativistic time delay*, ApJ 590, 683.
- Winn, J. N., Rusin, D. & Kochanek, C. S.: 2003, *Investigation of the possible third image and mass models of the gravitational lens PMN J1632–0033*, ApJ 587, 80.
- Wucknitz, O.: 2004, *LensClean revisited*, MNRAS 349, 1.
- Wucknitz, O., Biggs, A. D. & Browne, I. W. A.: 2004, *Models for the lens and source of B0218+357: a LensClean approach to determine H_0* , MNRAS 349, 14.
- York, T., Jackson, N., Browne, I. W. A., Wucknitz, O. & Skelton, J. E.: 2005, *The Hubble constant from the gravitational lens CLASS B0218+357 using the Advanced Camera for Surveys*, MNRAS 357, 124.
- Zhang, M., Jackson, N., Porcas, R. W. & Browne, I. W. A.: 2007, *A search for the third lensed image in JVAS B1030+074*, MNRAS 377, 1623.